Supplementary Information

Supplementary Figure 1

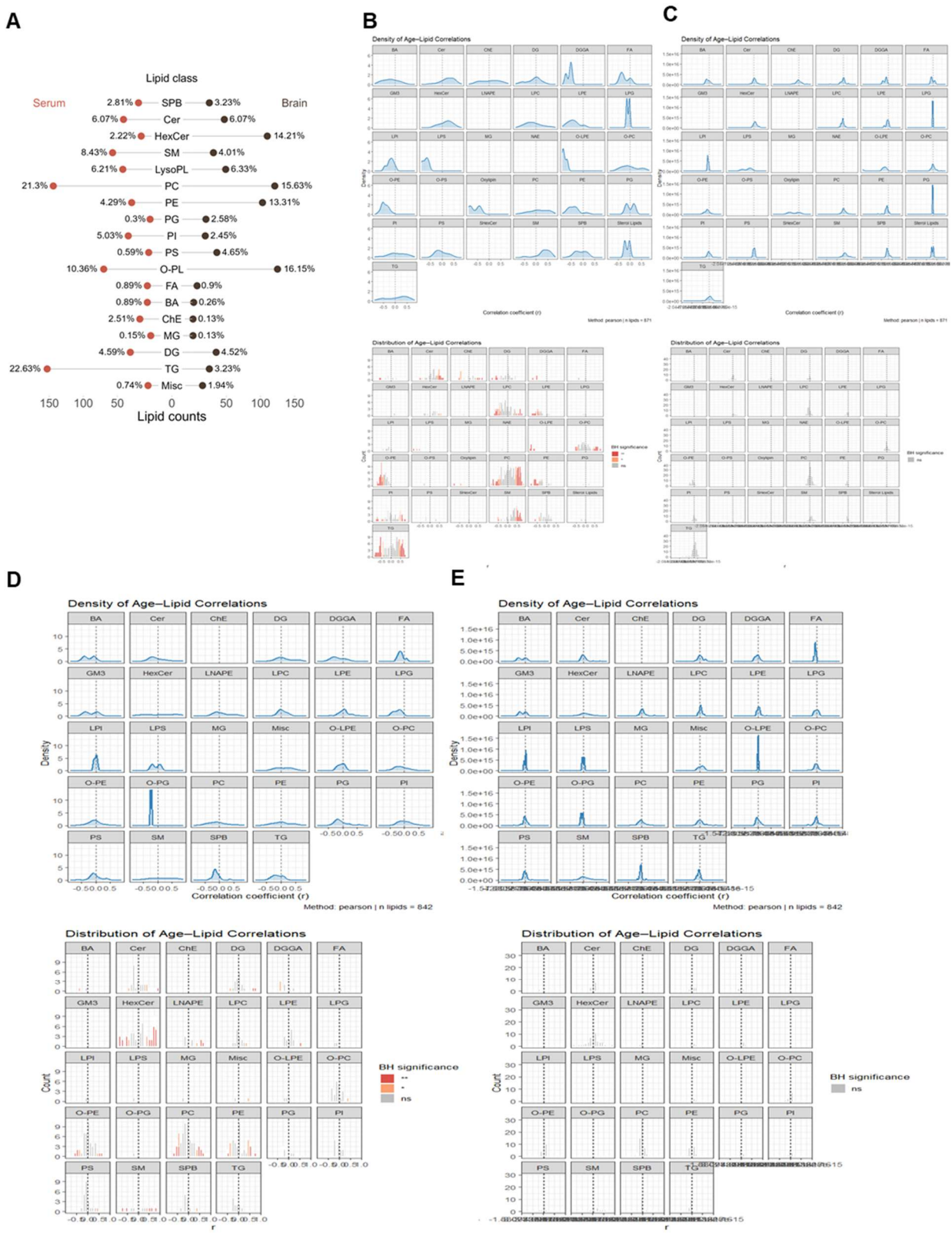


Figure. S1 Lipid-class composition and age-lipid associations in serum and brain before and after age adjustment.

(A) Distribution of lipid classes in serum (light brown) and brain (brown), shown as relative abundance (%) and the counts of annotated lipids per major lipid category. **(B-C)** Serum: density plots (top) show the distribution of Pearson correlation coefficients (r) between age and lipid species per lipid class, before **(B)** and after correction **(C)**. Bar plots (bottom) summarize the number of significant (red) and non-significant (gray) associations within each class following Benjamini-Hochberg (BH) adjustment. **(D-E)** Brain, as in B-C, before **(D)** and after **(E)** adjustment. Age was modeled as a continuous covariate, and its linear component was removed with limma::removeBatchEffect() while sex was retained in the design matrix (see Methods).

Supplementary Figure 2

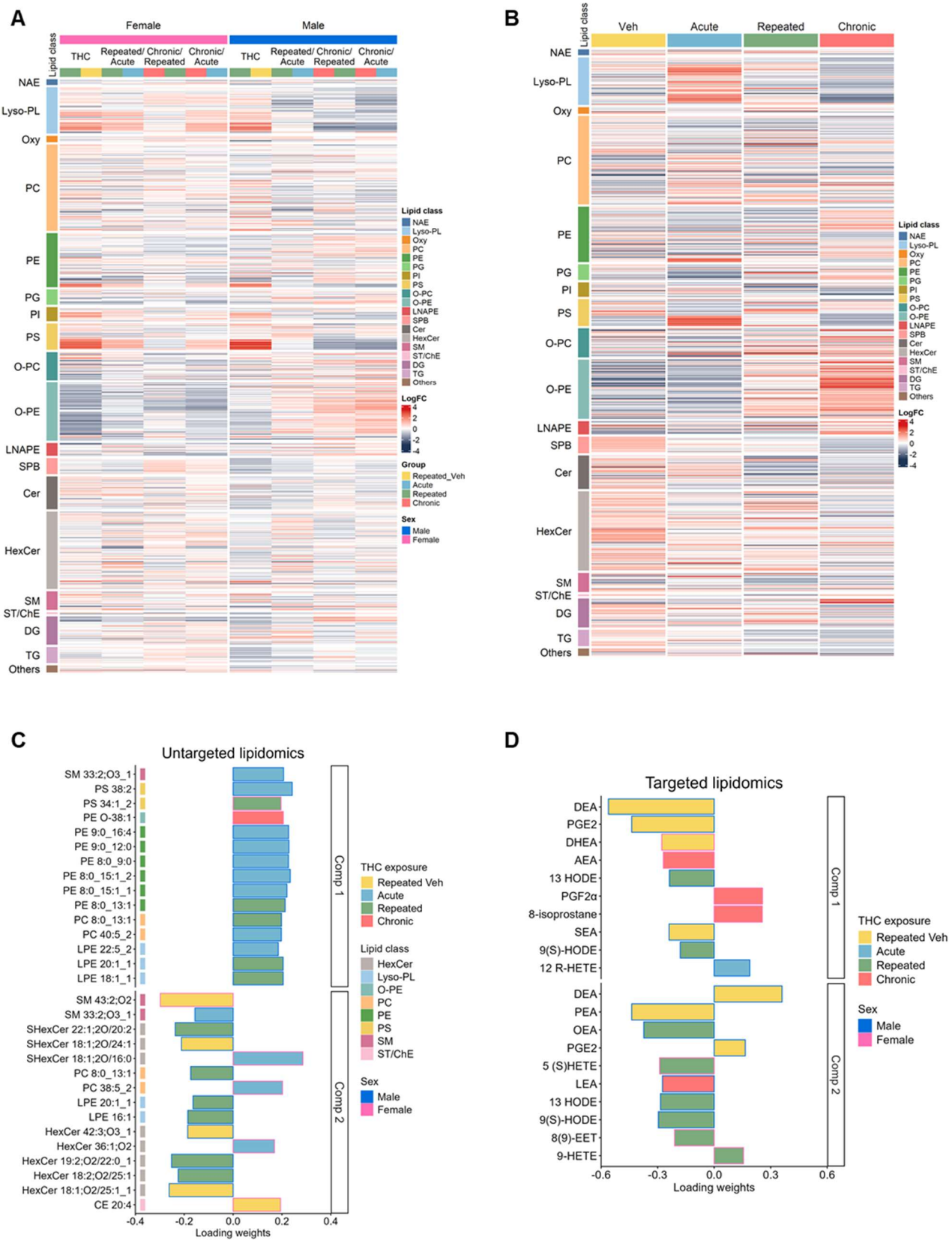


Figure. S2 Sex-dependent hippocampal lipidomic remodeling across THC exposure histories and the features driving multigroup separation.

(A) Heatmap of untargeted lipidomics showing global lipid abundance changes across THC exposure histories in females and males. Lipids are grouped by lipid class (left annotation), and samples are organized by exposure groups (THC: THC vs Veh, Repeated/Acute: Repeated vs Acute; Chronic/Repeated: Chronic vs Repeated; Chronic/Acute: Chronic vs Acute). Color intensity represents normalized log fold change (LogFC), with red indicating positive logFC and blue indicating negative LogFC. **(B)** Heatmap of lipid profiles across exposure groups (Vehicle, Acute, Repeated, Chronic), highlighting sex-specific (male vs female) remodeling patterns across lipid classes. **(C-D)** Loading weights of the features with the largest absolute loadings on components 1 and 2 of the multiblock sPLS-DA (DIABLO) model in **Fig. 2B**, for the untargeted **(C)** and targeted **(D)** lipidomics blocks. Bar fill indicates the exposure group and bar outline indicates the sex of the group with the highest median abundance of each feature. Colored tiles along the y-axis denote lipid class.

Supplementary Figure 3

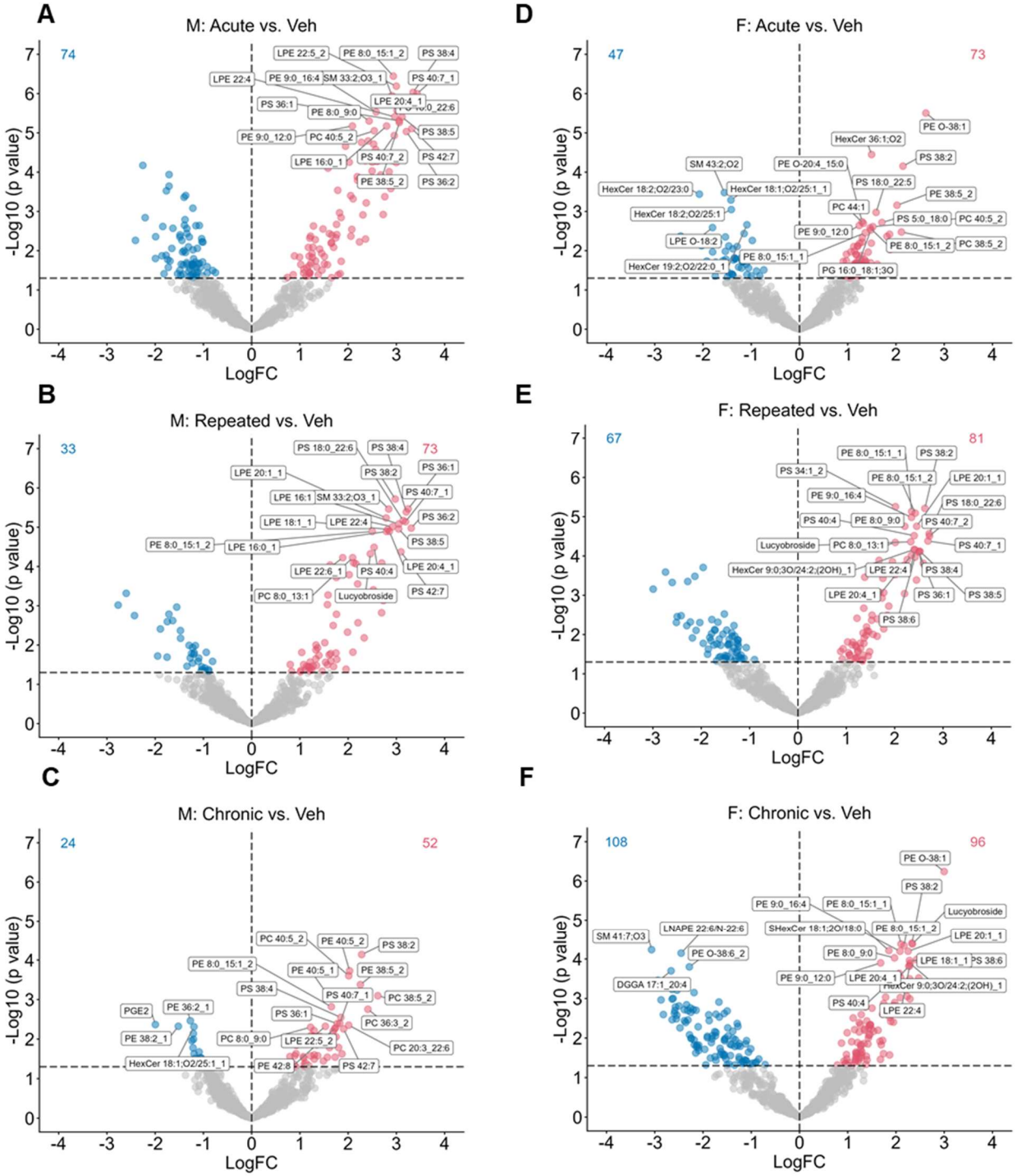


Figure. S3 Differential hippocampal lipid abundance after acute, repeated, and chronic THC exposure relative to vehicle.

Volcano plots showing differential lipid abundance between THC-exposed groups and vehicle controls in males (**A-C**) and females (**D-F**) across exposure paradigms: acute (**A, D**), repeated (**B, E**), and chronic (**C, F**). Each point represents an individual lipid species, plotted by log fold change (LogFC, x-axis) and statistical significance ($-\log_{10}$ p value, y-axis). Vertical dashed lines indicate zero fold change, and the horizontal dashed line indicates the significance threshold (p=0.05). Significantly increased and decreased lipids are shown in red and blue, respectively; non-significant species are shown in gray. The top 20 lipid species ranked by absolute log fold change are annotated. Numbers in the upper corners denote the total counts of significantly decreased (left, blue) and increased (right, red) lipids for each comparison. n = 5-6 animals per group.

Supplementary Figure 4

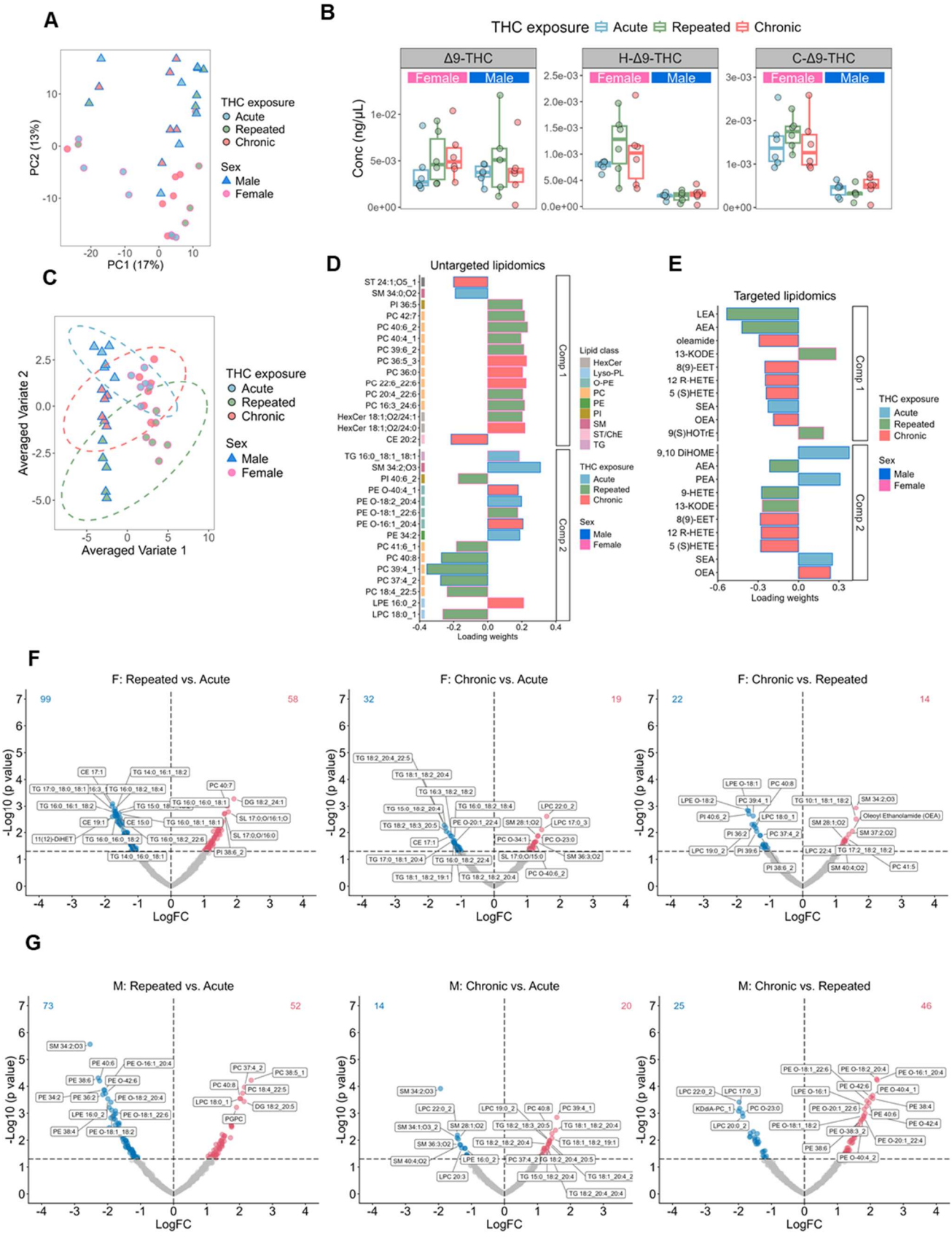


Figure.S4 Serum cannabinoid levels and sex-dependent serum lipidomic organization across THC exposure histories.

(A) Principal component analysis (PCA) of integrated serum lipidomics. Circles, females; triangles, males; colors, exposure history. **(B)** Targeted quantification of THC and metabolites (C-Δ9-THC, Δ9-THC, H-Δ9-THC) across exposure groups (Acute, Repeated, Chronic), stratified by sex. Boxplots show median and interquartile range (IQR); points represent individual animals. Group comparisons were performed using ANOVA followed by Tukey's post hoc test. $P < 0.05$ was considered statistically significant. No pairwise comparisons between exposure histories reached significance within either sex. **(C)** Averaged variate plot of the multiblock PLS-DA (DIABLO) model built on stability-selected features. **(D–E)** Loading weights of the top features on components 1 and 2 for the untargeted **(D)** and targeted **(E)** blocks; bar color indicates the group with the highest median abundance. **(F-G)** Volcano plots showing differential lipid abundance between exposure conditions in females **(F)** and males **(G)** across comparisons (repeated vs acute, chronic vs repeated, and chronic vs acute). Each point represents an individual lipid species, plotted by log fold change (LogFC, x-axis) and statistical significance ($-\log_{10}$ p value, y-axis). Vertical dashed lines indicate zero fold change, and the horizontal dashed line indicates the significance threshold ($p=0.05$). Significantly increased and decreased lipids are shown in red and blue, respectively; non-significant species are shown in gray. The top 20 lipid species ranked by absolute log fold change are annotated. Numbers in the upper corners denote the total counts of significantly decreased (left, blue) and increased (right, red) lipids for each comparison.

Supplementary Figure 5

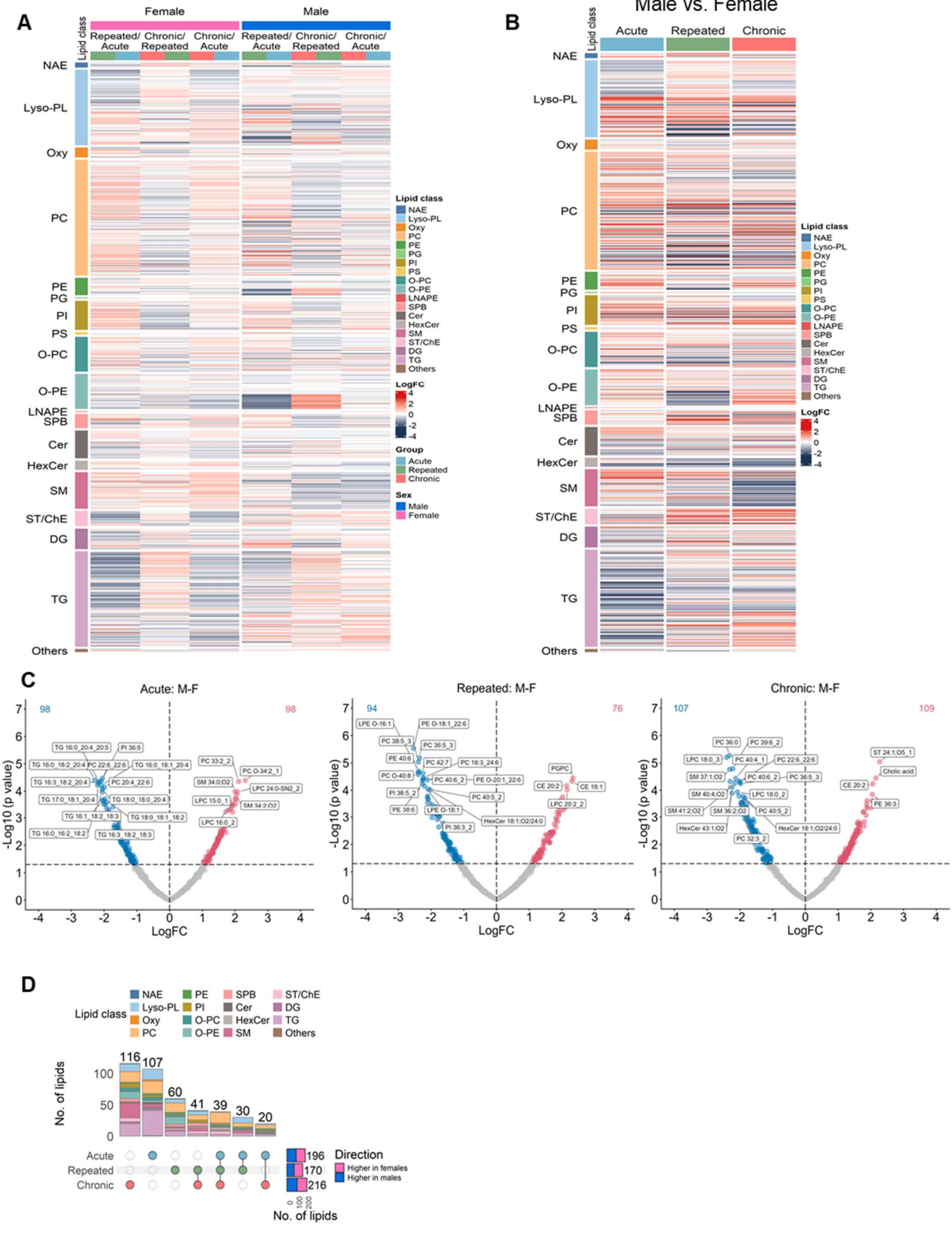


Figure.S5 Sex-dependent serum lipidomic remodeling across THC exposure revealed by global lipid profiles and key lipid drivers.

(A) Heatmap of untargeted lipidomics showing global lipid abundance changes across THC exposure conditions in females and males. Lipids are grouped by lipid class (left annotation), and samples are organized by exposure groups (Repeated/Acute: Repeated vs Acute; Chronic/Repeated: Chronic vs Repeated; Chronic/Acute: Chronic vs Acute). Color intensity represents normalized log fold change (LogFC), with red indicating positive logFC and blue indicating negative LogFC. **(B)** Heatmap of lipid profiles across exposure groups (Acute, Repeated, Chronic), highlighting sex-specific (male vs female) remodeling patterns across lipid classes. **(C)** Volcano plots of lipid abundance changes comparing male vs female (M-F) across exposure paradigms (acute, repeated, chronic). Each point represents an individual lipid species plotted by log fold change (LogFC) and statistical significance ($-\log_{10}$ p value). Significantly increased lipids are shown in red, decreased lipids in blue, and non-significant lipids in gray. The top 20 lipid species ranked by absolute log fold change are annotated. Numbers in the upper corners denote the total counts of significantly decreased (left, blue) and increased (right, red) lipids for each comparison. **(D)** UpSet plot of lipids differing by sex ($P < 0.05$) across exposure histories. Vertical bars give intersection sizes, with stacked colors showing lipid class; the dot matrix defines each intersection; horizontal bars give the total per exposure history.

Supplementary Figure 6 (Brain)

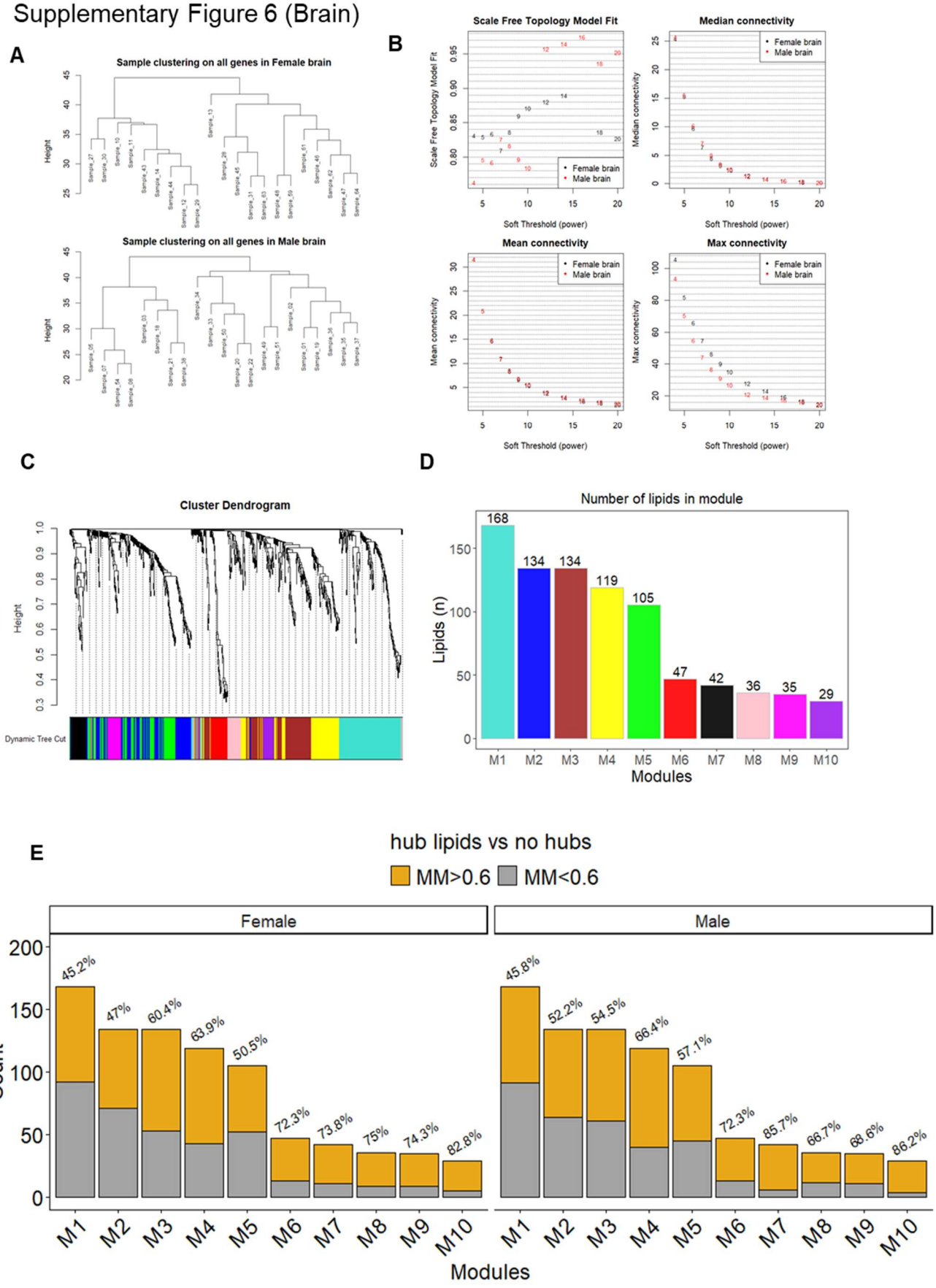


Figure.S6 Consensus WGCNA of the hippocampal lipidome.

(A) Hierarchical clustering dendrograms of samples based on lipid profiles in female (top) and male (bottom). Samples cluster without prominent outliers, indicating high data quality and suitability for network construction. **(B)** Soft-threshold selection: scale-free topology fit (R^2) and mean, median, and maximum connectivity across powers in each sex. $\beta = 12$ was selected ($R^2 = 0.973$ in females, 0.949 in males). **(C)** Cluster dendrogram of lipid modules identified by dynamic tree cutting (deepSplit = 4, minimum module size = 25, cutHeight = 0.995) based on topological overlap. Distinct modules (M1-M10) are indicated by color bars below the dendrogram, representing groups of co-expressed lipids with shared network structure. **(D)** Number of lipids within each identified module. Module sizes range from smaller modules (M10, 29 lipids) to large modules (M1, 168), reflecting heterogeneity in lipid network organization. **(E)** Distribution of hub versus non-hub lipids across modules in females (left) and males (right). Hub lipids are defined by high module membership ($MM \geq 0.6$, $P < 0.05$), while non-hub lipids have lower membership ($MM < 0.6$).

Supplementary Figure 7 (serum)

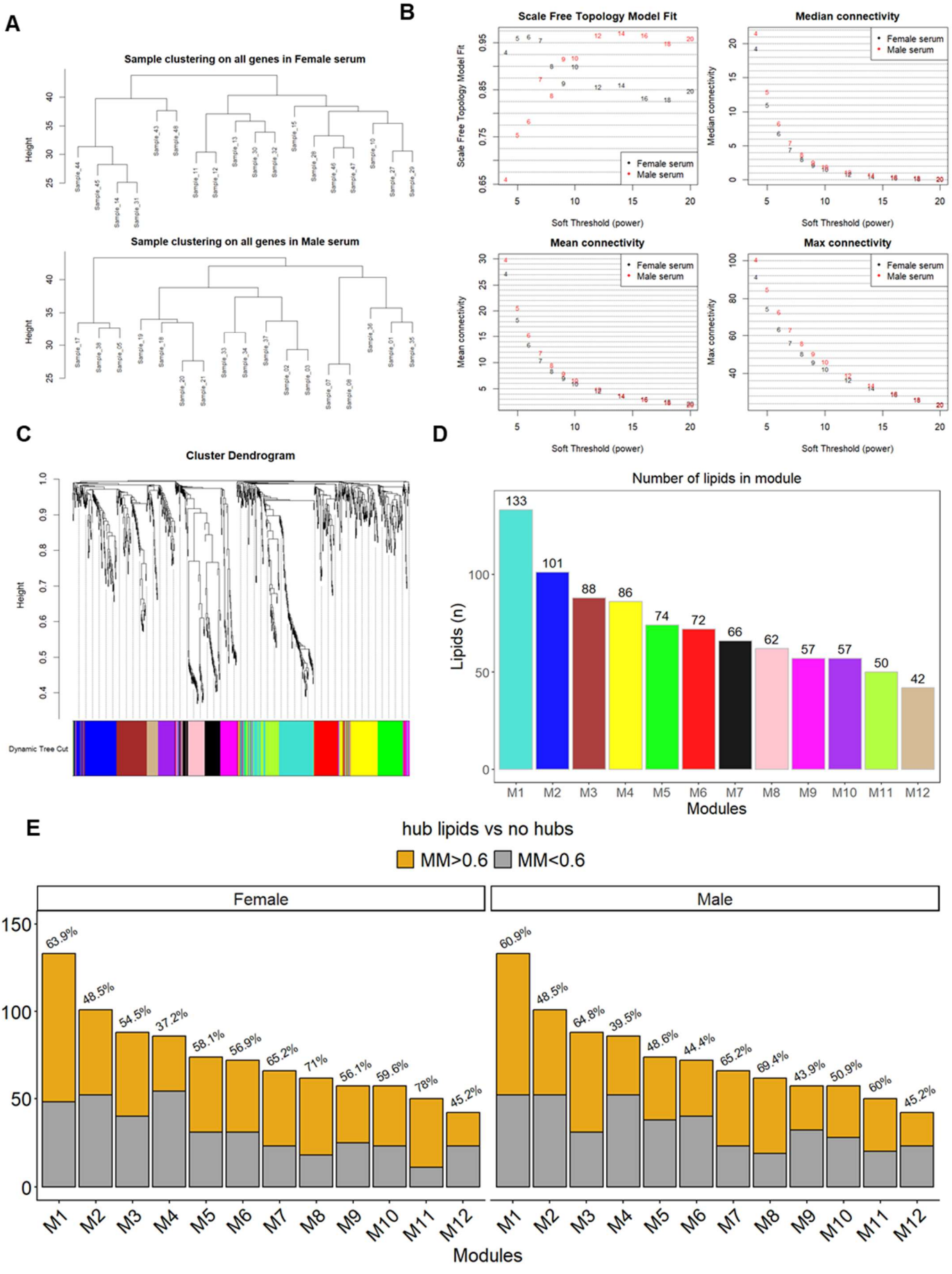


Figure.S7 Consensus WGCNA of the serum lipidome.

As in **Fig. S6**, for serum: **(A)** clustering of female (top) and male (bottom) serum samples. **(B)** $\beta = 10$ ($R^2 = 0.877$ in females, 0.903 in males). **(C)** Modules M1-M12 (minimum module size = 30). **(D)** Module sizes (M1, 133 lipids, to M12, 42). **(E)** Hub and non-hub lipids by sex.

Supplementary Figure 8

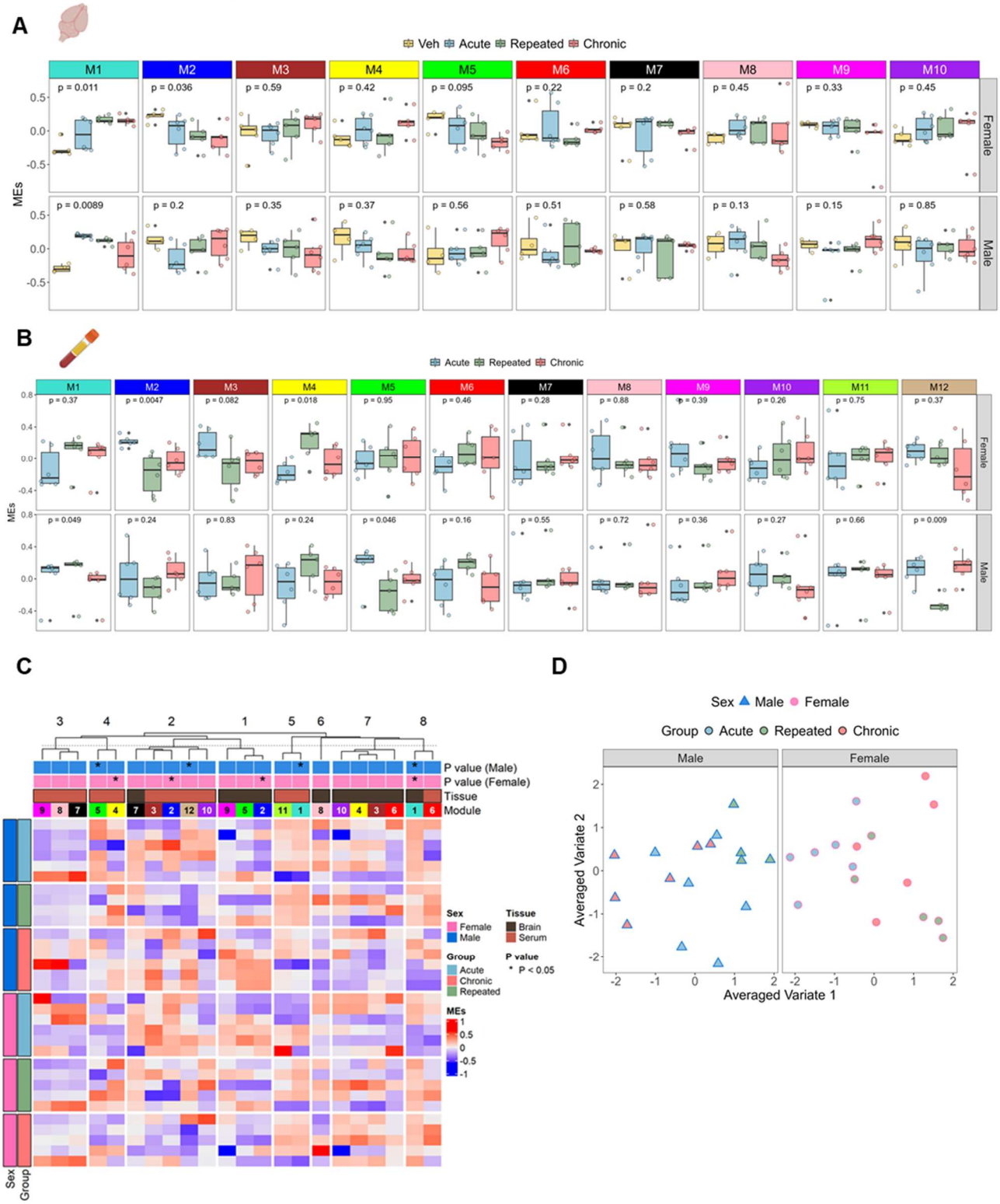


Figure. S8 Sex-dependent lipid module dynamics and cross-tissue coordination across THC exposure revealed by WGCNA and multivariate integration

(A) Boxplots of module eigengene (MEs) values for brain lipid modules (M1-M10) across THC exposure conditions (vehicle, acute, repeated, chronic) in females (top) and males (bottom). Each module represents a group of co-expressed lipids defined by WGCNA. Differences across exposure groups were evaluated using Kruskal–Wallis tests, with p values indicated for each module. **(B)** Boxplots of MEs for serum lipid modules (M1-M12) across exposure conditions in females (top) and males (bottom). **(C)** Heatmap of module eigengene (ME) values across all samples, clustered by hierarchical clustering. Samples are annotated by sex, tissue (brain vs serum), exposure group, and module. Color intensity (blue to red) reflects relative ME levels. Clustering reveals coordinated module variation with graded, rather than discrete, separation across exposure groups. Group differences were assessed using Kruskal-Wallis tests, with $P < 0.05$ (*) indicated (top row: male; second row: female). **(D)** DIABLO integration of selected brain and serum consensus module eigengenes, showing sample distribution across latent variables. Samples are colored by exposure condition and shaped by sex, with sex-stratified views illustrating partial separation driven by coordinated cross-tissue module signals, alongside substantial overlap between groups.

Supplementary Figure 9

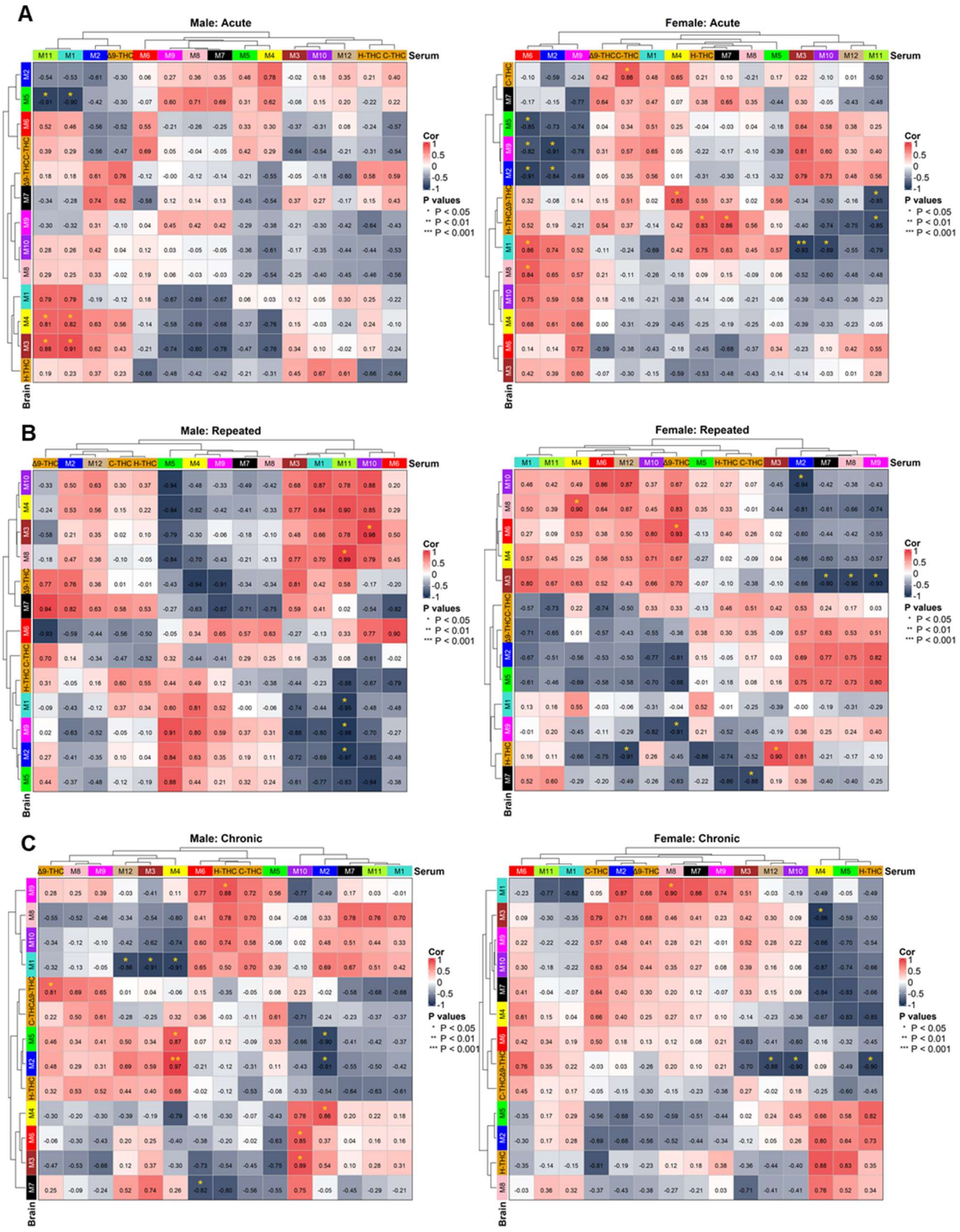


Figure. S9 Sex-specific brain-serum lipid module coupling across acute, repeated, and chronic THC exposure.

Heatmaps showing pairwise correlations between brain and serum lipid modules and THC metabolites across acute **(A)**, repeated **(B)**, and chronic **(C)** THC exposure**,** stratified by sex (male vs female). Each panel corresponds to a specific exposure condition and sex (Male: left; Female: right). Rows represent brain modules and brain THC metabolites, and columns represent serum features. Color intensity indicates Pearson correlation coefficients (r), with red representing positive correlations and blue representing negative correlations. Statistical significance is denoted by symbols (* $P < 0.05$, ** $P < 0.01$). Correlations computed within each exposure history and sex (n = 5-6).

Supplementary Figure 10

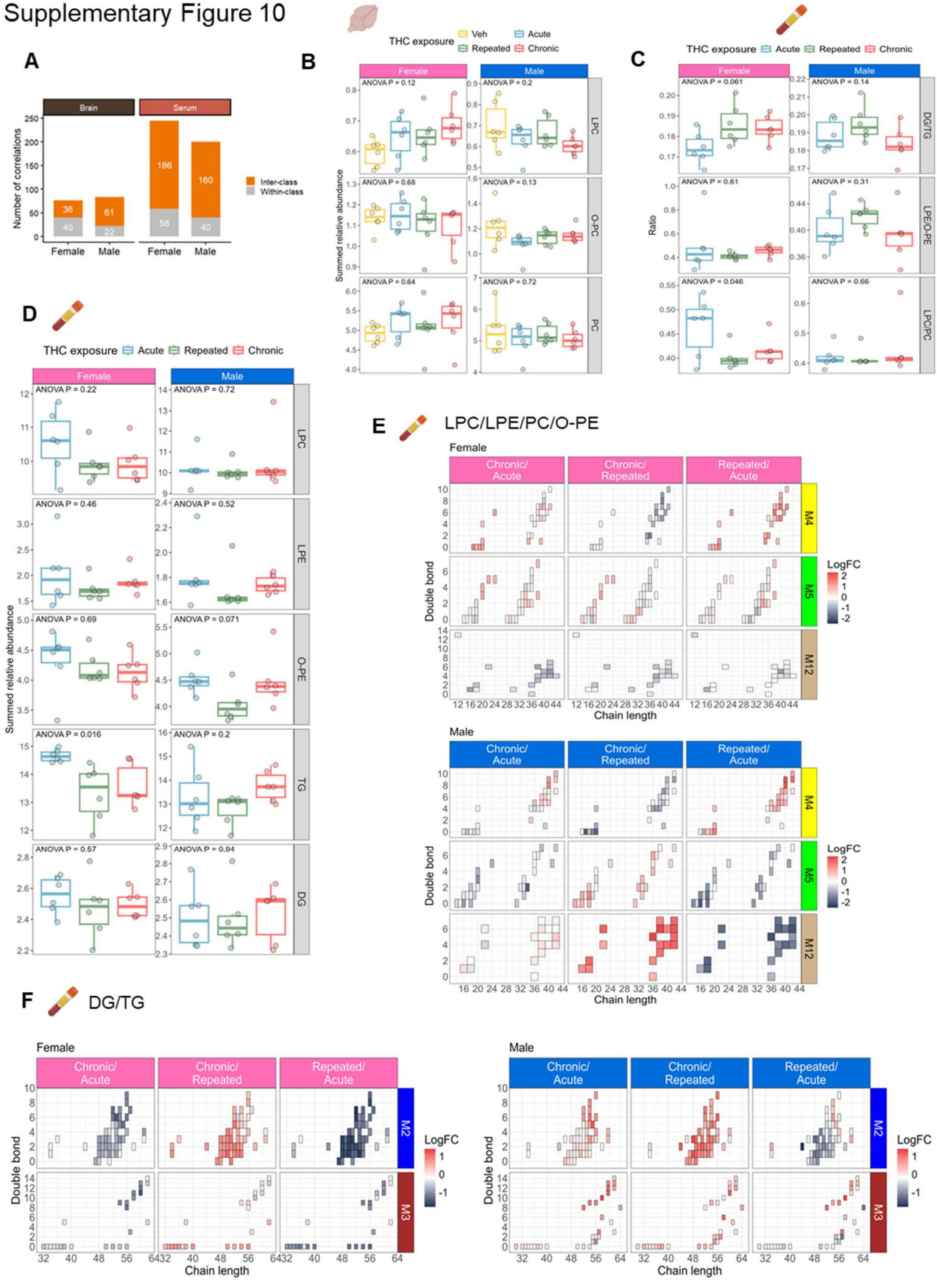


Figure. S10 Lipid correlation network summary, lipid-class sums, and structural maps of serum lipid modules across THC exposure history.

(A) (A) Summary of the Spearman correlation networks in **Fig. 3C-D**, giving the number of significant lipid–lipid correlations ($P < 0.05$, $|\rho| > 0.6$) between and within lipid classes in serum and hippocampus of females and males. Within-class correlations are counted here but were not displayed in **Fig. 3C-D**. **(B)** Summed relative abundance of LPC, O-PC, and PC species in the hippocampus of repeated vehicle (Veh), acute, repeated, and chronic groups, by sex. Each species was normalized before summation, so values reflect the average relative level of species within each class. **(C)** Ratios of summed relative abundance of DG/TG, LPE/O-PE and LPC/PC in serum after acute, repeated, and chronic THC exposure, by sex. **(D)** Summed relative abundance of LPC, LPE, O-PE, TG, and DG species in the serum of acute, repeated, and chronic groups, by sex. Each species was normalized before summation, so values reflect the average relative level of species within each class. **(E)** Structural maps of lysophospholipid and PC species (LPC, LPE, and PC) in the lysophospholipid/PI-enriched (M4) and lysophospholipid/PC-enriched (M5) serum modules, and of O-PE species in the O-PE-enriched serum module (M12). Maps are shown for females (upper) and males (lower) for repeated vs acute, chronic vs repeated, and chronic vs acute. **(F)** Structural map of TG species in the TG-enriched/related serum module (M2 and M3), as in **(E)**. In **(E)** and **(F)**, the x-axis is total fatty-acyl chain length and the y-axis is total number of double bonds. Each species is colored by log fold change (red, increased; blue, decreased). In **(B)** and **(D)**, boxplots show the median and interquartile range, with whiskers extending to 1.5 × IQR, and points are individual animals (n = 5-6 per group). P values are from one-way ANOVA across exposure groups within each sex. Serum was not collected from vehicle-treated animals, so serum comparisons are among exposure histories only.

Supplementary Figure 11

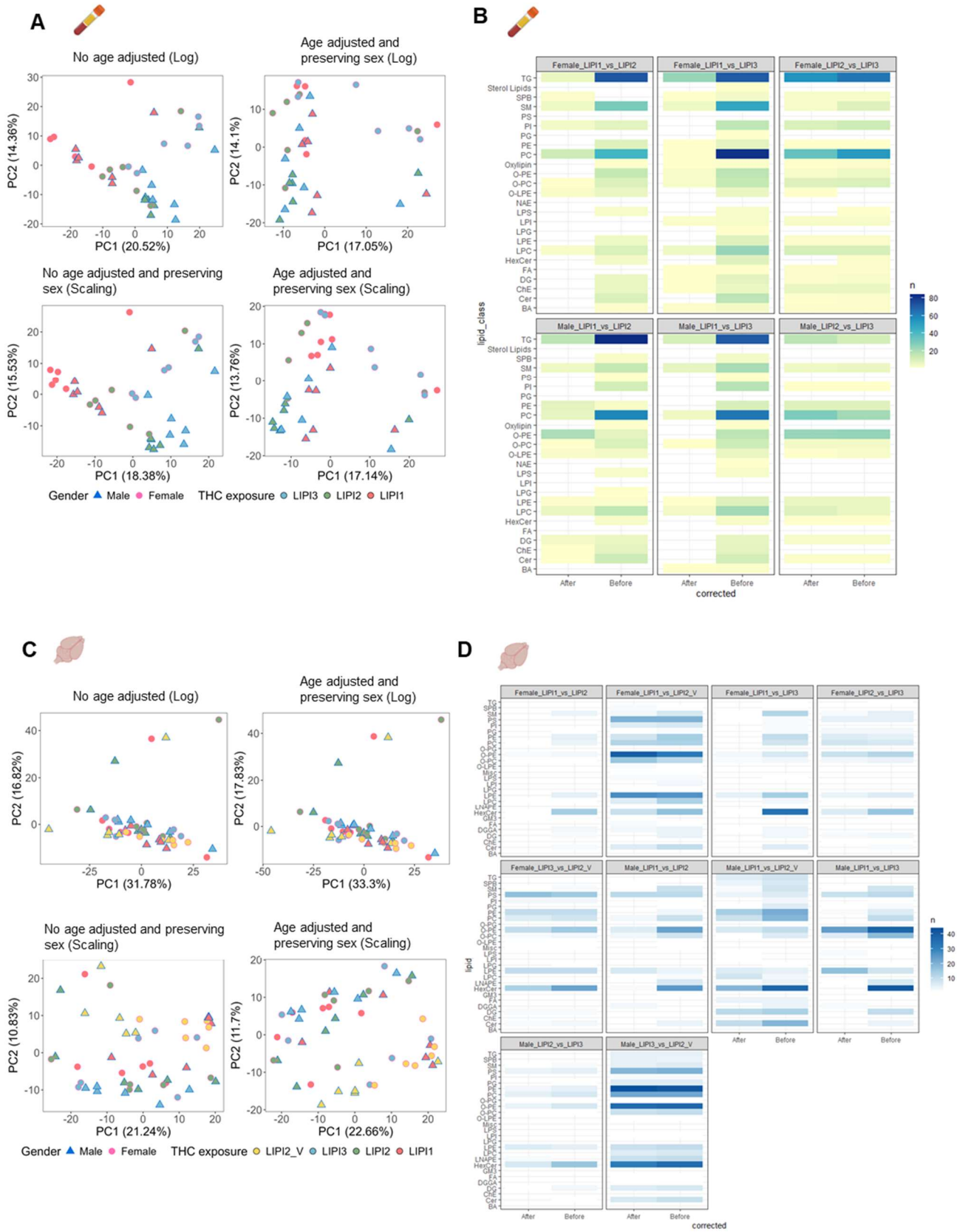


Figure. S11 Effect of age adjustment on the global structure of the serum and hippocampal lipidomes and on differential lipid results.

(A) Principal component analysis (PCA) of serum lipidomics under four processing conditions: without age adjustment, log-transformed data (top left); age-adjusted with sex preserved, log-transformed data (top right); without age adjustment, scaled data (bottom left); age-adjusted with sex preserved, scaled data (bottom right). Shape indicates sex (triangles, male; circles, female), and color indicates THC exposure history (acute, repeated, chronic). Percentages give the variance explained by each principal component. **(B)** Number of significantly altered serum lipids ($P < 0.05$) per lipid class in each pairwise comparison between exposure histories (chronic vs repeated, chronic vs acute, repeated vs acute), in females (top) and males (bottom). For each comparison, results without age adjustment (Before) and with age adjustment (After) are shown side by side. Color intensity indicates the number of significant lipids (n). **(C)** PCA of hippocampal lipidomics under the same four processing conditions as in **(A)**. Groups include repeated vehicle, acute, repeated, and chronic THC exposure. **(D)** Number of significantly altered hippocampal lipids ($P < 0.05$) per lipid class, before and after age adjustment. Comparisons include each THC exposure history vs repeated vehicle and the pairwise comparisons between exposure histories, in females and males. Age adjustment removed the linear effect of age, modeled as a continuous covariate, using limma::removeBatchEffect(), with sex retained in the design matrix. Scaled data were feature- and sample-centered after log transformation (see Methods). Differential analyses used limma moderated statistics; P values are unadjusted. n = 5-6 animals per group.

Supplementary Figure 12

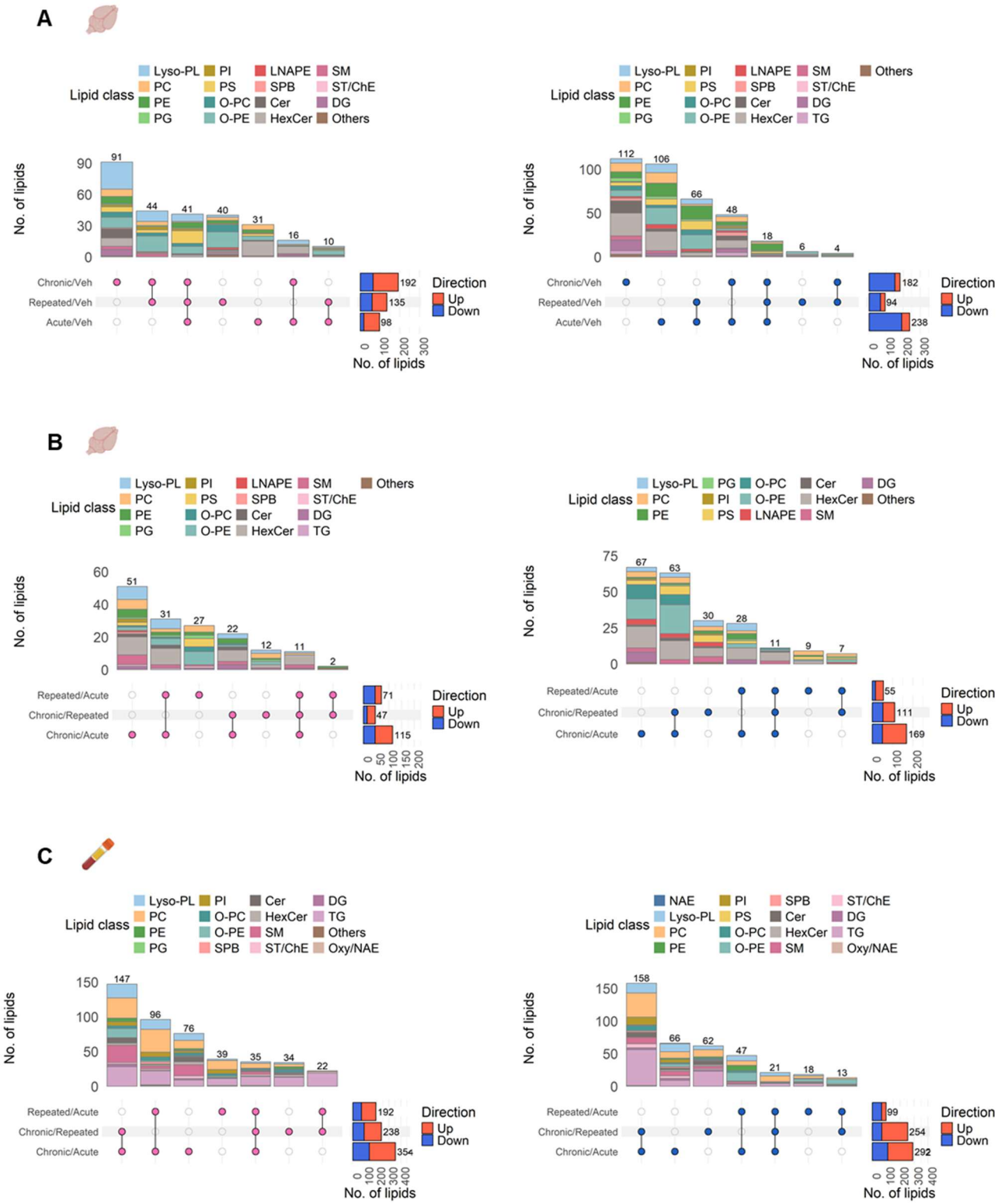


Figure S12. Differential lipid analyses without age adjustment. UpSet plots of lipids altered at P < 0.05 (unadjusted P values; limma moderated statistics) using log-transformed data without removal of the linear age trend**. (A)** Hippocampus, each THC exposure history vs repeated vehicle, in females (left) and males (right). **(B)** Hippocampus, pairwise comparisons among exposure histories. **(C)** Serum, pairwise comparisons among exposure histories. Vertical bars show intersection sizes, with stacked colors indicating lipid class; the dot matrix defines each intersection; horizontal bars give the total number of altered lipids per comparison, split into increased (red) and decreased (blue). n = 5–6 animals per group. Compare with age-adjusted results in **Fig. 2D-E** and **Fig. 3A**.

Supplementary Figure 13



Figure S13. Lipid class sums without age adjustment. Summed abundances of selected lipid classes and lysophospholipid ratios calculated from age-unadjusted data, in females and males. **(A)** LPE/O-PE and LPE/PE ratios in the hippocampus**. (B–D)** Hippocampal sums of O-PE, LPE, and PE **(B)**; PS and PI **(C)**; and O-PC, PC, and LPC **(D)** across vehicle, acute, repeated, and chronic THC exposure. **(E)** Serum sums of TG and DG across acute, repeated, and chronic THC exposure; serum was not collected from vehicle-treated animals. Lipid class sums were calculated after back-transforming log2 abundances. Boxplots show the median and interquartile range, with whiskers extending to 1.5 × IQR; points represent individual animals (n = 5-6 per group). P values are from one-way ANOVA across exposure groups within each sex. Age-adjusted results are shown in **Fig. 5C, E** and **Fig. S10B-D**.